A Dispersion Law for Virtually Imaged Phased-Array Spectral Dispersers Based on Paraxial Wave Theory

Shijun Xiao, *Student Member, IEEE*, Andrew M. Weiner, *Fellow, IEEE*, and Christopher Lin

***Abstract*—We derive the spectral dispersion law for the virtually imaged phased array (VIPA) based on paraxial wave theory using the Fresnel diffraction analysis. The validity of the dispersion law is verified by comparison with experiments. This spectral dispersion law is compared to a previous law based on plane wave theory. At small incident angles where the VIPA provides its largest spectral dispersion, the paraxial wave law provides a much better fit to the data than the plane wave law does.**

***Index Terms*—Optical devices, spectral dispersers, wavelength demultiplexers.**

I. Introduction

THE virtually imaged phased array (VIPA) was introduced recently as a new optical spectral disperser that provides several potential advantages over common diffraction gratings, including large angular dispersion, low polarization sensitivity, simple structure, low cost, and compactness. The application of the VIPA for wavelength division multiplexing (WDM) has been demonstrated [1], [2]. VIPA designs with reduced low insertion loss and crosstalk were reported in [3]. Chromatic dispersion compensation [4]–[6] using the VIPA in an optical pulse-shaping setup has also been demonstrated. Another interesting application of the VIPA spectral disperser is in Fourier transform pulse shaping [7]. Finally, the VIPA can potentially be used as part of a direct space-to-time pulse-shaping setup for wide-band arbitrary millimeter-wave generation [8], [9].

The VIPA can be viewed as a modified Fabry–Perot etalon. It typically consists of two glass plates, of which the back or the transmission side is coated with a partially reflectivity film (e.g., $\geq$95%); the front or entry side is coated with an almost 100% reflective film except in a window area, which is uncoated or antireflection (AR) coated, and the laser enters the VIPA through this window area. If the etalon cavity is filled with air, it is called an air-spaced VIPA; otherwise, if it is filled with some glass of refractive index n_r, it is called a solid VIPA. A collimated laser source is focused with a cylindrical lens into the VIPA etalon. Due to the high reflectivity of the VIPA etalon, the laser beam experiences multiple reflections back and forth, and the multiple reflections result in multiple diverging output beams from the transmission plate. These output beams interfere with each other to form collimated propagating beams with different output angles depending on the wavelength. The name comes from the device operating as if there were multiple virtual sources interfering with each other as in a phased array. As in any phased array, the direction of the output beam depends on the phase difference between the array elements (virtual sources). Since this phase difference is frequency-dependent, the direction of the output beam also varies with frequency, i.e., the VIPA functions as a spectral disperser (Fig. 1.).

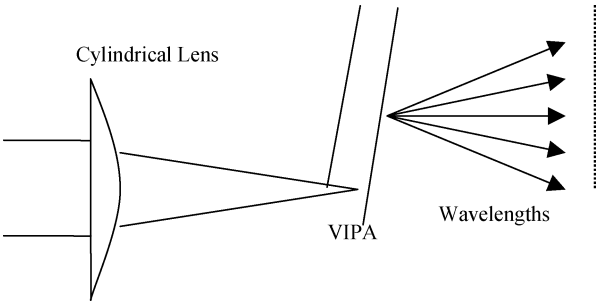

Fig. 1. VIPA spectral disperser.

The essential function of the VIPA is as a spectral disperser, i.e., different wavelengths are dispersed to different output angles. In this sense, the VIPA is related to the Lummer–Gehrke plate and other classical optical multiple beam interference devices [10], [11]. It is also related in this sense to the arrayed-waveguide grating [12], where multiple delay paths result in frequency-dependent angular dispersion. Although the structure of the VIPA physically resembles that of a Fabry–Perot interferometer [11], the function is quite different; the classical Fabry–Perot acts as a frequency-dependent transmission and reflection filter, but not as an angular disperser.

A spectral dispersion law for the VIPA was derived using plane wave theory in a recent paper by Vega [13]. This previous dispersion law was tested using relatively large incident angles ($> 5^\circ$) and was found to match well with experimental data. Here we present a modified dispersion law that is an analytic result from the Fresnel diffraction theory, which takes into account paraxial waves and Gaussian beams. Theoretically, the modified law strongly departs from the previous law for small incident angles ($< 5^\circ$) on the VIPA, and the difference decreases for large incident angles $\geq 5^\circ$. This validity of our new law is confirmed by experiments focusing on the small incident angle range where the theories differ most noticeably.

The remainder of this paper is structured as follows. Section II contains our theoretical derivation of the modified spectral dispersion law for the VIPA. Section III is the comparison between

Manuscript received October 23, 2003; revised December 23, 2003. This work was supported in part by the National Science Foundation under Grant 0100949-ECS and by the Army Research Office under Grant DAAD19-01-1-0427.

S. Xiao and A. M. Weiner are with the School of Electrical and Computer Engineering, Purdue University, West Lafayette, IN 47907-1285 USA (e-mail: sxiao@ecn.purdue.edu; amw@ecn.purdue.edu).

C. Lin is with the Avanex Corporation, Fremont, CA 94538 USA (e-mail: Christopher_Lin@avanex.com).

Digital Object Identifier 10.1109/JQE.2004.825210

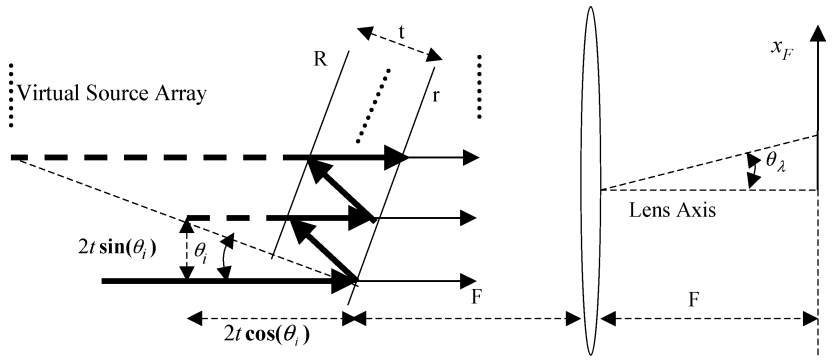

Fig. 2. VIPA spectral disperser geometry, showing the transverse and longitudinal distances between neighboring virtual sources.

our new law based on paraxial wave theory with the previous plane wave theory. Section IV discusses the experimental results and the fit with the theory. Section V presents the conclusion.

II. Theoretical Derivation

Without loss of generality, the air-spaced VIPA is assumed in the following derivation. We assume a Gaussian input beam and ignore any reshaping of the input beam as it is coupled into the etalon. This should be reasonable as long as the focused spot size of the input beam to the VIPA is optimized. As described in the introduction, the VIPA can be viewed as an array of virtual sources (Fig. 2). For the nth virtual source, the beam profile is taken to be a Gaussian with an exponentially decreasing intensity as follows:

$$E_n(x) = (Rr)^n E_0 \exp\left(-\frac{(x-\Delta x_n)^2}{{w_0}^2}\right) \quad n = 0, 1, 2 \ldots. \tag{1}$$

Rr is the reflectivity product of the highly reflective coating and the partially reflective coating, $w_0 = (\lambda f/\pi W)$ is the beam radius of the incident beam into the etalon, where W is the radius of the collimated beam prior to the cylindrical lens, f is the focal length of cylindrical lens, and λ is the wavelength. The transverse displacement of the nth virtual source is $\Delta x_n = n2t\sin(\theta_i)$ (Fig. 2). The nth virtual source is displaced longitudinally by an amount $\Delta z_n = n2t\cos(\theta_i)$ with respect to the waist of the first incident beam spot. We also assume that the incident beam comes to a waist on the back surface of the VIPA, which is taken to be located at the front focal plane of the focusing lens. Finally, we assume that the receiver is on the back focal plane of the focusing lens, so we would have symmetric demultiplexing transmission spectra lineshape with minimal linewidth [14].

The modified spatial Fourier transform by a thin lens [15], [16] (the relation between the field on the object plane before the lens and the field on the back focal plane after the lens analysis) is obtained through a Fresnel diffraction analysis with the result

$$E_{\text{out}}(x_F, \lambda) \propto \exp(-ikd)\exp\left[-i\frac{k}{2F}\left(1-\frac{d}{F}\right){x_F}^2\right] \times \int_{-\infty}^{\infty} E_{\text{in}}(x)\exp\left(\frac{ikx_F x}{F}\right)dx \tag{2}$$

where d is the distance of the object plane to the lens, F is the focal length of the lens, and $k = \omega/c = 2\pi/\lambda$ and is the wave vector.

According to the virtual sources model described above, the object plane-lens distance d in (2) should be represented by $d_n = F + \Delta z_n$ for the nth virtual source. As it will become clear from the following derivation, only the relative displacements of the sources Δz_n will be needed to determine the interference between the sources; the assumption that the first spot is at the front focal plane is unnecessary.

The result of applying (2) to the nth source is

$$E_{\text{out}_n}(x_F, \lambda) \propto \exp(-ik\Delta z_n)\exp\left(i\frac{k\Delta z_n}{2F^2}{x_F}^2\right) \times \int_{-\infty}^{\infty} E_n(x)\exp\left(\frac{ikx_F x}{F}\right)dx \tag{3}$$

Substituting in for $E_n(x)$ using (1), we have

$$E_{\text{out}_n}(x_F, \lambda) \propto (Rr)^n \exp\left(-\frac{f^2}{F^2}\frac{{x_F}^2}{W^2}\right) \times \exp\left(-i\frac{4n\pi t\cos(\theta_i)}{\lambda}\right) \times \exp\left(i\frac{4n\pi t\sin(\theta_i)x_F}{\lambda F}\right) \times \exp\left(i\frac{2n\pi t\cos(\theta_i){x_F}^2}{\lambda F^2}\right). \tag{4}$$

The total field at the back focal plane is obtained by summing over the virtual sources as follows:

$$E_{\text{out}}(x_F, \lambda) \propto \exp\left(-\frac{f^2}{F^2}\frac{{x_F}^2}{W^2}\right) \times \sum_{n=0}^{N}\left\{(Rr)^n \exp\left(-i\frac{4n\pi t\cos(\theta_i)}{\lambda}\right) \times \exp\left(i\frac{2n\pi t\cos(\theta_i){x_F}^2}{\lambda F^2}\right) \times \exp\left(i\frac{4n\pi t\cos(\theta_i)x_F}{\lambda F}\right)\right\}. \tag{5}$$

If we assume that N is large enough (valid for a device with sufficiently large transverse aperture or equivalently for suffi-

ciently small incident angles) so that we can perform an infinite series sum, the simplified output field is

$$E_{\text{out}}(x_F,\lambda) \propto \exp\left(-\frac{f^2}{F^2}\frac{{x_F}^2}{W^2}\right) \times \frac{1}{1-Rr\exp\left(-i\frac{4\pi t\cos(\theta_i)}{\lambda}+i\frac{4\pi t\sin(\theta_i)x_F}{\lambda F}+i\frac{2\pi t\cos(\theta_i){x_F}^2}{\lambda F^2}\right)}. \tag{6}$$

The intensity distribution function is

$$I_{\text{out}}(x_F,\lambda) \propto |E_{\text{out}}(x_F,\lambda)|^2 \propto \exp\left(-\frac{2f^2{x_F}^2}{F^2W^2}\right) \times \frac{1}{(1-Rr)^2+4(Rr)\sin^2\left(\frac{k\Delta}{2}\right)} \tag{7}$$

where $\Delta = 2t\cos(\theta_i) - ((2t\sin(\theta_i)x_F)/F) - ((t\cos(\theta_i){x_F}^2)/F^2)$

With a narrow-band input, the output spatial intensity has a Gaussian roll-off function along the lateral x_F direction on the back focal plane. As a function of wavelength, the VIPA interferometer demonstrates an Airy–Lorentzian lineshape for any fixed value of x_F.

The transmission peak wavelengths satisfy the constructive interference phase-matching condition

$$k\Delta = k\left[2t\cos(\theta_i) - \frac{2t\sin(\theta_i)x_F}{F} - \frac{t\cos(\theta_i){x_F}^2}{F^2}\right] = 2m\pi. \tag{8}$$

Under the Fresnel paraxial approximation, $(x_F)/(F) \approx \theta_\lambda$ (this ignores third or higher orders of the output angle). As a result, the phase-matching equation can be written as

$$k\left[2t\cos(\theta_i) - 2t\sin(\theta_i)\theta_\lambda - t\cos(\theta_i){\theta_\lambda}^2\right] = 2m\pi. \tag{9}$$

Equation (9) is the spectral dispersion law for the VIPA.

One important consequence of the dispersion law is the free spectral range (FSR). The FSR derived from the paraxial dispersion law (9) is

$$\text{FSR} = \frac{c}{2t\cos(\theta_i) - 2t\sin(\theta_i)\theta_\lambda - t\cos(\theta_i){\theta_\lambda}^2}. \tag{10}$$

Using a second-order Taylor series approximation of the FSR as a function of output angle, we have

$$\text{FSR} = \frac{c}{2t\cos(\theta_i)}\left\{1+\tan(\theta_i)\theta_\lambda + \left[\frac{1}{2}+\tan^2(\theta_i)\right]{\theta_\lambda}^2\right\}. \tag{11}$$

Another direct and important consequence of the spectral dispersion law is the relation between the peak output wavelength and the output angle, i.e., λ_p versus θ_λ, which provides more information than the FSR.

The relation derived from the paraxial dispersion law (9) is

$$\Delta\lambda = \lambda_p - \lambda_0 = -\lambda_0\left[\tan(\theta_i)\theta_\lambda + \frac{1}{2}{\theta_\lambda}^2\right] \tag{12}$$

where $m\lambda_0 = 2t\cos(\theta_i)$.

The angular dispersion factor from (12) is

$$\frac{d\theta_\lambda}{\frac{d\lambda_p}{\lambda_0}} = -\frac{1}{\tan(\theta_i)+\theta_\lambda}. \tag{13}$$

Although our derivation focuses on the air-spaced VIPA, it is also applicable to the solid VIPA with small modifications. The corresponding equations for the solid VIPA with refractive index n_r are

$$k\left[2tn_r\cos(\theta_{\text{in}}) - 2t\tan(\theta_{\text{in}})\cos(\theta_i)\theta_\lambda - t\cos(\theta_{\text{in}}){\theta_\lambda}^2/n_r\right] = 2m\pi \tag{14}$$

where $n_r\sin(\theta_{\text{in}}) = \sin(\theta_i)$ (Snell's Law), and θ_{in} is the internal angle inside the solid etalon as a result of refraction.

The relation between wavelength and the output angle from the paraxial law is expressed by

$$\Delta\lambda = \lambda_p - \lambda_0 = -\lambda_0\left[\frac{\tan(\theta_{\text{in}})\cos(\theta_i)}{n_r\cos(\theta_{\text{in}})}\theta_\lambda + \frac{1}{2}{\theta_\lambda}^2/n_r^2\right] \tag{15}$$

where $m\lambda_0 = 2tn_r\cos(\theta_{\text{in}})$.

The angular dispersion factor from (15) is

$$\frac{d\theta_\lambda}{\frac{d\lambda_p}{\lambda_0}} = -\frac{1}{\frac{\sin(2\theta_i)}{2\left[{n_r}^2-\sin^2(\theta_i)\right]}+\theta_\lambda/{n_r}^2}. \tag{16}$$

All of these equations are reduced to that of the air-spaced VIPA by setting the refractive index $n_r = 1$, which is the air-spaced VIPA.

Please note that the dispersion law for the VIPA remains the same even if N is finite. The reason is that the constructive interference phase-matching condition simply requires that the relative phase difference between two neighboring terms in (5) is a multiple of 2π.

III. Comparison With the Previous Plane-Wave Dispersion Law

It is important to compare our dispersion law derived from paraxial wave theory with previously proposed dispersion laws of the VIPA. The only detailed previous dispersion law for the VIPA was published by Vega and Weiner [13] using a plane wave theory. In case of an air-spaced VIPA, the formula from the plane wave theory is

$$\omega\frac{2t}{c}\left\{\frac{1}{\cos\theta_i} - \tan(\theta_i)\sin(\theta_i+\theta_\lambda)\right\} = 2m\pi. \tag{17}$$

Using the Fresnel paraxial approximation, (17) is reduced to the following expression:

$$k\left[2t\cos(\theta_i) - 2t\sin(\theta_i)\theta_\lambda + t\tan(\theta_i)\sin(\theta_i){\theta_\lambda}^2\right] = 2m\pi. \tag{18}$$

We also obtain the FSR from (18) as

$$\text{FSR} = \frac{c}{2t\cos(\theta_i)}\left[1+\tan(\theta_i)\theta_\lambda + \frac{1}{2}\tan^2(\theta_i){\theta_\lambda}^2\right]. \tag{19}$$

By comparing (11) and (19), we see that the FSR in the paraxial wave theory has a stronger quadratic variation with the output angle. This is important because the first-order term that

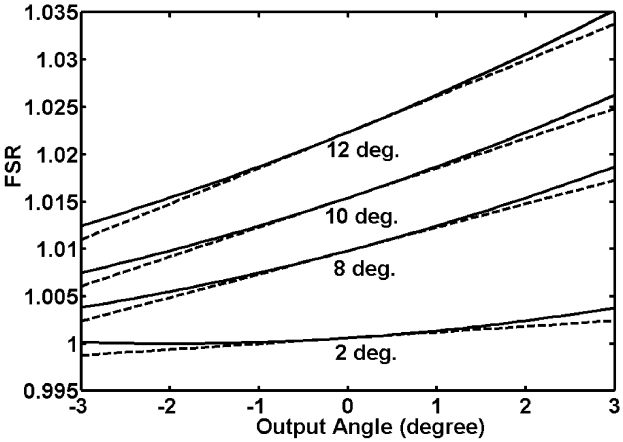

Fig. 3. FSR, normalized by $c/2t$, as a function of output angle for different incident angles: 2°, 8°, 10°, and 12°. The solid lines stand for the paraxial law, and the dashed lines stand for the plane wave law.

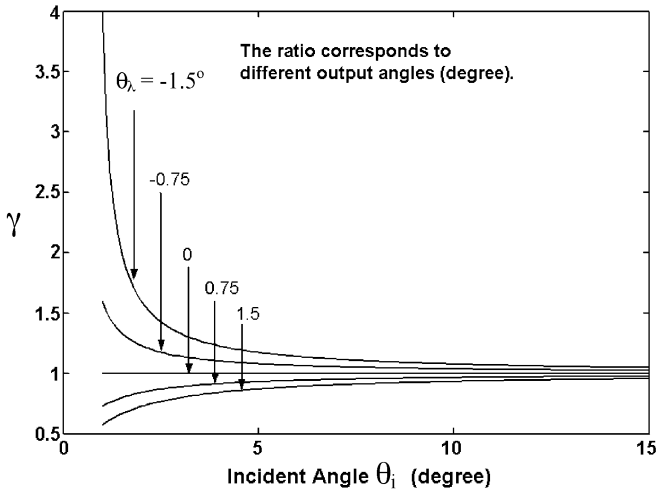

Fig. 4. Ratio γ between the wavelength shifts from the two theories—see (21). γ is plotted as a function of input angle θ_i with output angle θ_λ as a parameter.

is the same in both theories becomes very small for small input angles, where the spectral dispersion is larger. A theoretical comparison for (11) and (19) is shown in Fig. 3. There is an obvious difference for the two theories.

The relation between the wavelength and the output angle from (18) is

$$\Delta\lambda = \lambda_p - \lambda_0 = -\lambda_0 \left[\tan(\theta_i)\theta_\lambda - \frac{1}{2}\tan^2(\theta_i){\theta_\lambda}^2\right] \quad (20)$$

where $m\lambda_0 = 2t\cos(\theta_i)$.

It is obvious that the spectral dispersion law differs in the term that is quadratic in the output angle. In order to have a closer look at this difference, we examine the ratio γ between the $\Delta\lambda$ from (20) with the $\Delta\lambda$ from (12) as follows:

$$\gamma = \frac{\tan(\theta_i)\theta_\lambda - \tan^2(\theta_i)\frac{{\theta_\lambda}^2}{2}}{\tan(\theta_i)\theta_\lambda + \frac{{\theta_\lambda}^2}{2}} \approx \frac{1 - \tan(\theta_i)\tan\frac{(\theta_\lambda)}{2}}{1 + \frac{1}{2}\frac{\tan(\theta_\lambda)}{\tan(\theta_i)}} \quad (21)$$

Note that the paraxial approximation $\theta_\lambda \approx \tan(\theta_\lambda)$ is used in (21).

Theoretical curves are plotted in Fig. 4. γ departs significantly from unity for small incident angles ($< 5°$); the difference in the quadratic terms in the two theories is important in this regime. On the other hand, this quadratic term has little effects for incident angles ($\geq 10°$) so that $\gamma \approx 1$. Here the term that is first order in the output angle dominates, so the two theories yield the same result. In the region where there is a significant output power ($|\theta_\lambda| \leq 1.5°$ in experiments here), the paraxial approximation is always valid, which means it is justified and interesting to do a paraxial theory and to compare its result with the results from plane wave theory simplified according to the paraxial approximation. We need to set the VIPA at small incident angles ($< 5°$) to clearly measure the quadratic relations of (12); otherwise, we have an approximately linear relation, which has been confirmed in the work by Vega *et al.* [13].

In addition, for a solid VIPA, the dispersion law proposed by using the plane wave theory in [13] is

$$\omega\frac{2t}{c}\left[\frac{n_r}{\cos(\theta_{\text{in}})} - \tan(\theta_{\text{in}})\sin(\theta_i + \theta_\lambda)\right] = 2m\pi \quad (22)$$

In the paraxial approximation, this equation becomes

$$2kt\left[n_r\cos(\theta_{\text{in}}) - \tan(\theta_{\text{in}})\cos(\theta_i)\theta_\lambda + \frac{1}{2}\tan(\theta_{\text{in}})\sin(\theta_i){\theta_\lambda}^2\right] = 2m\pi. \quad (23)$$

The relation between wavelength and the output angle from the plane wave law is expressed by

$$\begin{aligned}\Delta\lambda &= \lambda_p - \lambda_0 \\ &= -\lambda_0\left[\frac{\tan(\theta_{\text{in}})\cos(\theta_i)}{n_r\cos(\theta_{\text{in}})}\theta_\lambda - \frac{1}{2}\frac{\tan(\theta_{\text{in}})\sin(\theta_i)}{\cos(\theta_{\text{in}})}{\theta_\lambda}^2\right].\end{aligned} \quad (24)$$

Comparing (15) with (24), the difference is similar to that with the air-spaced VIPA: the paraxial theory shows a much stronger quadratic dependence on the output angle than does the plane wave theory.

IV. Experiments and Data Fitting

Since the case of large incident angles is carefully studied in the plane wave theory [13], we perform our experiment with small incident angles when the second-order effect is strongest. We confine our experiments to the air-spaced VIPA.

The VIPA spectral dispersion testing setup is plotted in Fig. 5. An air-spaced VIPA with a nominal FSR of 100 GHz corresponding to $t = 1.5$ mm is used. A collimated beam (beam radius 1.2 mm) from an amplified spontaneous emission (ASE) source is injected into the VIPA etalon after cylindrical lens focusing (cylindrical lens with either 60 mm or 300 mm in our experiment). The VIPA is placed on a fine rotation stage. A thin spherical lens with 180-mm focal length is placed around one focal length away behind the VIPA. The thin lens converts

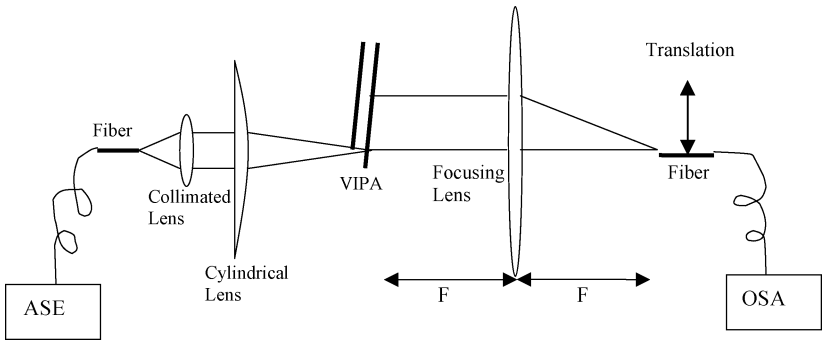

Fig. 5. Experimental setup for the VIPA spectral disperser measurements. ASE is an amplified spontaneous emission source. OSA is an optical spectrum analyzer with a spectral resolution of 0.01 nm.

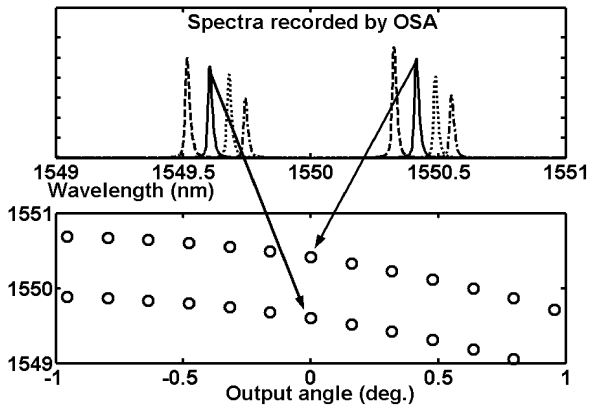

Fig. 6. Sample of the raw data (top) and an illustration of its use in plotting in wavelength versus output angle (bottom). Different line styles in the top plot correspond to different transverse positions in the output plane.

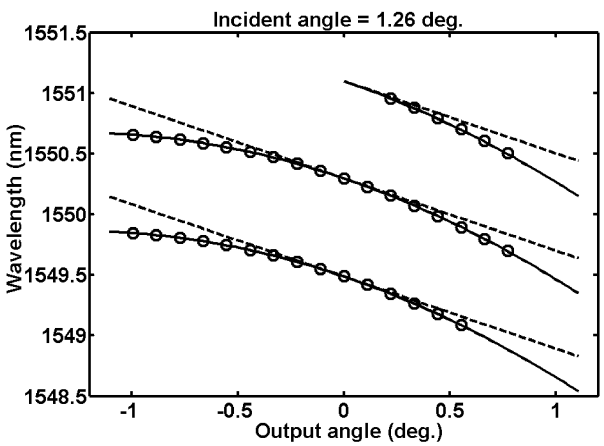

Fig. 7. Theoretical fit for the dispersion data using an input cylindrical lens of 300-mm focal length and a spherical lens of $F = 250$ mm. The beam radius at the VIPA input is $\sim$120 um. The circles are experimental data, the solid lines are fits using paraxial wave dispersion law, and the dashed lines are fits using plane wave dispersion law.

the angular dispersion into spatial dispersion on the back focal plane. A single-mode fiber is used to sample the light at the back focal plane. The fiber can be translated transversely along the x_F dimension on the back focal plane so that we can measure the peak output wavelength at different spatial positions. The receiver is connected to an optical spectrum analyzer (OSA) with 0.01-nm spectral resolution. In the setup, the relative shift of the incident angles can be controlled precisely up to 0.01°, but it is difficult to directly obtain the absolute incident angles. The zero output angle position is calibrated by finding the position with maximum power using a tunable laser source when the VIPA is removed from the setup.

Groups of data are taken to demonstrate the validity of the paraxial dispersion law. A group of dispersion data is taken at a small initial incident angle, and then other several groups of data are taken for different increasing incident angles, for which the relative shifts of the incident angle are precisely known. From these dispersion data, we plot families of wavelength versus output angle curves for different incident angles. An example of the spectra and dispersion data plots is shown in Fig. 6. The different line types in the spectra represent the fiber position, demonstrating the function of spectral dispersion. The different horizontal curves in the lower plot correspond to different diffraction orders of the VIPA. One interesting application of our paraxial dispersion theory is for fitting the thickness of the VIPA etalon. The thickness of the etalon is important because it determines the FSR, which often must be matched to a specified wavelength spacing. In a set of dispersion data showing wavelength versus output angle for a fixed incident angle, the neighboring dispersion curves have the two reference wavelengths that satisfy the following equations:

$$m\lambda_{01} = 2t\cos(\theta_i) \tag{25}$$

$$(m+1)\lambda_{02} = 2t\cos(\theta_i). \tag{26}$$

The combination of (25) and (26) yields

$$t = \frac{1}{2\cos(\theta_i)}\frac{\lambda_{01}\lambda_{02}}{\lambda_{01}-\lambda_{02}}. \tag{27}$$

After we use the data to fit the incident angles, we can calculate the thickness of the VIPA. An average thickness of 1.485 mm is obtained using all sets of dispersion data. This matches well with the nominal VIPA thickness (1.5 mm).

We have the following parameters to fit: the focal length of the thin lens and the incident angle. We have fit the dispersion data using our paraxial dispersion law. We start with the first incident angle and fit the data corresponding to a certain single order m according to (12). Here we fit values of the focal length (only a very small deviation from the nominal value) and the first incident angle. Then (12) is used to fit all remaining data both from the same incident angle and all of the other shown incident angles without any further adjustable parameters. The re-

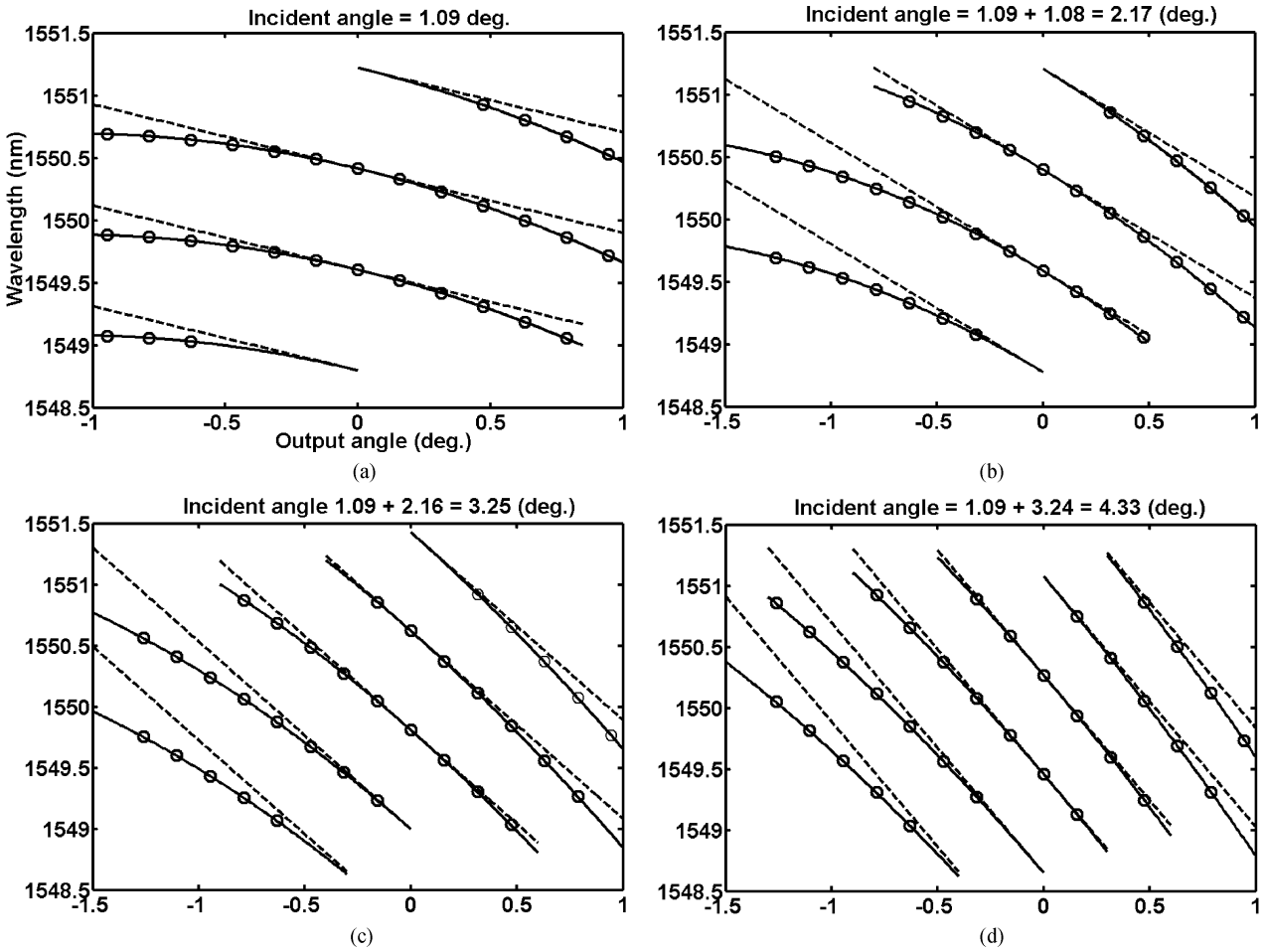

Fig. 8. Theoretical fits for the dispersion data using an input cylindrical lens of 60-mm focal length and a spherical lens with $F = 180$ mm. The incident angles are 1.09°, 2.17°, 3.25°, and 4.33° for (a)–(d), respectively. The beam radius at the VIPA input is $\sim$24 μm. The circles are experimental data, the solid lines are fits using paraxial wave dispersion law, and the dashed lines are fits using plane wave dispersion law.

sults are shown in Figs. 7 and 8. The circles are the experimental data, the solid curves are the fitting using our paraxial dispersion law, and the dashed curves are fits from the plane wave dispersion law of [13]. The dispersion law from the paraxial wave theory matches essentially perfectly with the experimental data according to the plot, which confirms the validity of our theory. The plot also clearly demonstrates the difference between fits using the paraxial and plane wave theories; for small incident angles as tested here, the paraxial theory gives an obvious better fit.

Figs. 7 and 8 are for different cylindrical focusing conditions, which yield two different focused beam radii: $\sim$24 and $\sim$120 μm at the VIPA. It is interesting to notice that the dispersion law is independent of the beam focusing condition into the VIPA etalon, as was proved in our previous derivation.

V. Conclusion

The VIPA spectral dispersion law has been studied both in theory and experiment. A dispersion law is derived using paraxial wave theory and validated by experiments. Our spectral dispersion law includes a strong second-order term relating wavelength and output angle, which differs from a previous plane wave theory [13] for the VIPA spectral disperser. Our results should be useful for the design of demultiplexers and other devices based on VIPA spectral dispersers.

References

[1] M. Shirasaki, "Large angular dispersion by a virtually imaged phased array and its application to a wavelength demultiplexer," *Opt. Lett.*, vol. 21, pp. 366–368, 1996.

[2] ——, "Virtually Imaged Phased Array (VIPA) Having Air Between Reflecting Surfaces," U.S. Patent 5 969 866, Oct. 19, 1999.

[3] ——, "Virtually imaged phased array with graded reflectivity," *IEEE Photon. Technol. Lett.*, vol. 11, pp. 1443–1445, 1999.

[4] ——, "Chromatic-dispersion compensator using virtually imaged phased array," *IEEE Photon. Technol. Lett.*, vol. 9, pp. 1598–1560, 1997.

[5] ——, "Compensation of chromatic dispersion and dispersion slope using a virtually imaged phased array," in *Proc. Optical Fiber Communication Conf.*, 2001, paper TuS1-3.

[6] ——, "Optical Apparatus Which Uses a Virtually Imaged Phased Array to Produce Chromatic Dispersion," U.S. Patent 20 030 021 046, Jan. 30, 2003.

[7] A. M. Weiner, "Femtosecond pulse shaping using spatial light modulators," *Rev. Sci. Instrum.*, vol. 71, pp. 1929–1960, 2000.

[8] S. Xiao, J. D. McKinney, and A. M. Weiner, "Photonic radio-frequency arbitrary waveform generation using a virtually-imaged phase-array (VIPA) direct space-to-time pulse shaper at 1.55 μm", to be presented at Conf. Laser and Electro Optics (CLEO).

[9] J. D. McKinney, D. E. Leaird, and A. M. Weiner, "Millimeter-wave arbitrary waveform generation with a direct space-to-time pulse shaper," *Opt. Lett.*, vol. 27, pp. 1345–1347, 2002.

[10] O. Lummer and E. Gehrcke, *Ann. D. Physik*, vol. 10, pp. 457–477, 1903.

[11] M. Born and E. Wolf, *Principles of Optics*. Cambridge, U.K.: Cambridge Univ., 1999, pp. 359–386.
[12] D. E. Leaird, S. Shen, A. M. Weiner, A. Sugita, S. Kamei, M. Ishii, and K. Okamoto, "Generation of high-repetition-rate WDM pulse trains from an arrayed-waveguide grating," *IEEE Photon. Technol. Lett.*, vol. 13, pp. 221–223, Mar. 2001.
[13] A. Vega, A. M. Weiner, and C. Lin, "Generalized grating equation for virtually-imaged phased-array spectral dispersers," *Appl. Opt.*, vol. 42, no. 20, pp. 4152–4155, July 2003.
[14] S. Xiao, A. M. Weiner, and C. Lin, "Spatial chirp effect in virtually-imaged phased-array wavelength demultiplexers," in *Proc. Conf. Laser and Electro Optics (CLEO)*, Baltimore, MD, June 1–6, 2003, CWP6.
[15] J. W. Goodman, *Introduction to Fourier Optics*. San Francisco, CA: McGraw-Hill, 1968, pp. 77–96.
[16] H. A. Haus, *Waves and Fields in Optoelectronics*. Englewood Cliffs, NJ: Prentice-Hall, 1984, pp. 81–107.

Shijun Xiao (S'04) was born in Chengdu, China, in 1979. He received the B.S. degree in electronics from Beijing University, Beijing, China, in 2001, and the M.S.E.C.E. degree in electrical and computer engineering from Purdue University, West Lafayette, IN, in 2003, where he is currently working toward the Ph.D. degree in electrical and computer engineering.

His current research area includes optical signal processing and pulse shaping, optical hyperfine-WDM/CDMA communications, and radio frequency (RF) photonics.

Mr. Xiao is a student member of the IEEE Lasers and Electro-Optics Society and the Optical Society of America. He received a two-year Andrews Fellowship from Purdue University for two years.

Andrew M. Weiner (S'84–M'84–SM'91–F'95) received the Sc.D. degree in electrical engineering from the Massachusetts Institute of Technology (MIT), Cambridge, in 1984.

From 1979 through 1984, he was a Fannie and John Hertz Foundation Graduate Fellow at MIT. In 1984, he joined Bellcore, at that time one of the premier research organizations in the telecommunications industry. In 1989, he was promoted to Manager of Ultrafast Optics and Optical Signal Processing. He joined Purdue University, West Lafayette, IN, in 1992 as a Professor of Electrical and Computer Engineering and is currently the Scifres Distinguished Professor of Electrical and Computer Engineering. From 1997 to 2003, he served as the ECE Director of Graduate Admissions. His research focuses on ultrafast optical signal processing and high-speed optical communications. He is especially well known for pioneering the field of femtosecond pulse shaping, which enables generation of nearly arbitrary ultrafast optical waveforms according to user specification. He has published four book chapters and over 120 journal articles. He has been author or coauthor of over 200 conference papers, including approximately 60 conference invited talks, and has presented over 50 additional invited seminars at universities or industry. He holds five U.S. patents.

Prof. Weiner is a Fellow of the Optical Society of America. He has been the recipient of numerous awards for his research, including the Hertz Foundation Doctoral Thesis Prize (1984), the Adolph Lomb Medal of the Optical Society of America (1990), awarded for pioneering contributions to the field of optics made before the age of thirty, the Curtis McGraw Research Award of the American Society of Engineering Education (1997), the International Commission on Optics Prize (1997), the IEEE Lasers and Electro-Optics Society (LEOS) William Streifer Scientific Achievement Award (1999), the Alexander von Humboldt Foundation Research Award for Senior U.S. Scientists (2000), and the inaugural Research Excellence Award from the Schools of Engineering at Purdue (2003). He has served on or chaired numerous research review panels, professional society award committees, and conference program committees. In 1988–1989, he served as an IEEE LEOS Distinguished Lecturer. He was General Co-Chair of the 1998 Conference on Lasers and Electro-Optics, Chair of the 1999 Gordon Conference on Nonlinear Optics and Lasers, and Program Co-chair of the 2002 International Conference on Ultrafast Phenomena. In addition, he has served as an Associate Editor for IEEE JOURNAL OF QUANTUM ELECTRONICS, IEEE PHOTONICS TECHNOLOGY LETTERS, and *Optics Letters*. He has served as an elected member of the Board of Governors of IEEE LEOS from 1997 to 1999 and as Secretary/Treasurer of IEEE LEOS from 2000 to 2002. He is currently a Vice President (representing IEEE LEOS) of the International Commission on Optics (ICO).

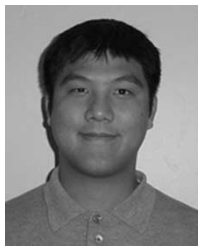

Christopher Lin received the B.S. and M.Eng. degrees in electrical engineering and computer science and the B.S. degree in economics from the Massachusetts Institute of Technology, Cambridge, in 2000.

Since graduating, he has been with Avanex Corporation, Fremont, CA, where he is currently a Product Development Manager. He has worked on the design and simulation of passive optical components for optical communications systems including multiplexers, interleavers, and chromatic dispersion compensators.